

Luogufengite: A new nano-mineral of Fe₂O₃ polymorph with giant coercive fieldHUIFANG XU^{1,*}, SEUNGYEOL LEE¹, AND HONGWU XU²¹NASA Astrobiology Institute, Department of Geoscience, University of Wisconsin-Madison, Madison, Wisconsin 53706, U.S.A.²Earth and Environmental Sciences Division, Los Alamos National Laboratory, Los Alamos, New Mexico 87545, U.S.A.

ABSTRACT

Luogufengite, Al-bearing ϵ -Fe₂O₃, is a new member of Fe₂O₃ polymorphs discovered in late Pleistocene basaltic scoria from the Menan Volcanic Complex nearby Rexburg, Idaho. It is an oxidation product of Fe-bearing basaltic glass at high temperature and is associated with maghemite and hematite. Luogufengite is an euhedral or semi-euhedral nano-mineral with its crystal size ranging from ~20 to ~120 nm. The mineral has a space group of *Pna*2₁; its unit-cell parameters refined from synchrotron X-ray powder diffraction pattern are $a = 5.0647(3)$, $b = 8.7131(6)$, $c = 9.3842(5)$ Å, and $Z = 4$ (calculated density = 4.905 g/cm³) with the doubled hexagonal (ABAC) packing of oxygen atoms. The eight strongest lines of the measured X-ray diffraction pattern [$d(\text{Å})/I(hkl)$] are: 3.197(27.3)(022); 2.945(29.1)(013); 2.708(100)(122); 2.437(35.8)(131); 1.716(24.4)(204); 1.507(40.7)(135); and 1.458(37.2)(330). The empirical formula is Fe_{1.71}Al_{0.24}Mg_{0.02}Ti_{0.03}O₃. The crystals display (110) twins with twin boundaries of (110), (100), and (130) due to their pseudo-hexagonal symmetry. Luogufengite is an important mineral that records paleomagnetism of volcanic rocks because of its large magnetic coercivity. This unique magnetic property of the mineral may explain the observed unusually high-remanent magnetization in some igneous and metamorphic rocks and even martian rocks with high-remanent magnetization. Some intergrowths of magnetite with ilmenite exsolution lamellae or hematite with magnetite lamellar precipitates have luogufengite-like 2D crystalline characteristics with the doubled hexagonal packing at the interface between cubic and rhombohedral structures. Luogufengite-like nano-domains at the magnetite/hematite interfaces might be responsible for the large coercive field of lodestones that are partially oxidized magnetite with hematite micro-precipitates.

Keywords: Luogufengite, hematite, maghemite, scoria, nano-mineral, remanent magnetization, coercive field, lodestone

INTRODUCTION

The new mineral luogufengite, a Fe₂O₃ polymorph analogous to the synthetic ϵ -Fe₂O₃, was discovered in late Pleistocene basaltic scoria from the Menan Volcanic Complex nearby Rexburg, Idaho. Powder X-ray diffraction (XRD) and high-resolution transmission electron microscopy (HRTEM) were used to determine its crystal structure and chemical composition. There are five known crystalline polymorphs of Fe₂O₃ to date: hematite (α -Fe₂O₃), maghemite (γ -Fe₂O₃), luogufengite (ϵ -Fe₂O₃), β -Fe₂O₃ (synthetic) (Zboril et al. 1999), and ζ -Fe₂O₃ (synthetic) (Tucek et al. 2015). Luogufengite is a dark brown nano-mineral—an intermediate polymorph between maghemite and hematite (Tronc et al. 1998; Machala et al. 2011; Lee and Xu 2016). Synthetic ϵ -Fe₂O₃ phase has a broad range of applications due to its unusual magnetic properties (e.g., giant coercive field, ferromagnetic resonance, and coupled magneto-electrics) (Jin et al. 2004; Gich et al. 2005; Tucek et al. 2010). The coercive field ($H_c = 2.0$ T) of ϵ -Fe₂O₃ nano-crystals is much larger than those of oxide-based commercial magnets of BaFe₁₂O₁₉ ($H_c = 0.64$ T) and Co-ferrites ($H_c = 0.74$ T) (Jin et al. 2004; Kohout et al. 2015).

In this paper, the crystal structure, composition, and mineral association of luogufengite are presented. There is a previous study on the mixture of ϵ -Fe₂O₃ and magnetite nano-crystals in subcellular phytoferritin of a plant (McClean et al. 2001). However, the published electron diffraction pattern (Fig. 2d in the paper) does not support the presence of ϵ -Fe₂O₃. Herein, we describe a natural ϵ -Fe₂O₃ (luogufengite) that occurs in basaltic scoria. The name has been approved by Commission on New Minerals, Nomenclature and Classification (CNMNC) of the International Mineralogical Association (IMA 2016-005) (Xu and Lee 2016). The mineral was named after a Chinese mineralogist, Professor Luo Gufeng (born in 1933), who has passionately taught crystallography and mineralogy at Nanjing University of China for more than 50 years. Luogufengite has been deposited in the collection of the Geology Museum of the Department of Geoscience, University of Wisconsin-Madison, with specimen numbers UWGM 2341, UWGM 2342, and UWGM 2343.

SAMPLES AND METHODS

Scoria samples containing luogufengite were collected from the Menan Volcanic Complex, Rexburg, Idaho. The Menan Volcanic Complex consists of broad, flat volcanoes, formed by low-viscosity eruptions, with tholeiitic basalts dominating the surface exposures (Hackett and Morgan 1988; Russell and Brisbin 1990). The formation of scoria was related to the interaction of external water with the late-stage (late Pleistocene) eruption in the center of the Menan complex (Hackett and Morgan 1988; Russell and Brisbin 1990). The scoria generally resulted from rapid vesicula-

* E-mail: hfxu@geology.wisc.edu

Special collection papers can be found online at <http://www.minsocam.org/MSA/AmMin/special-collections.html>.

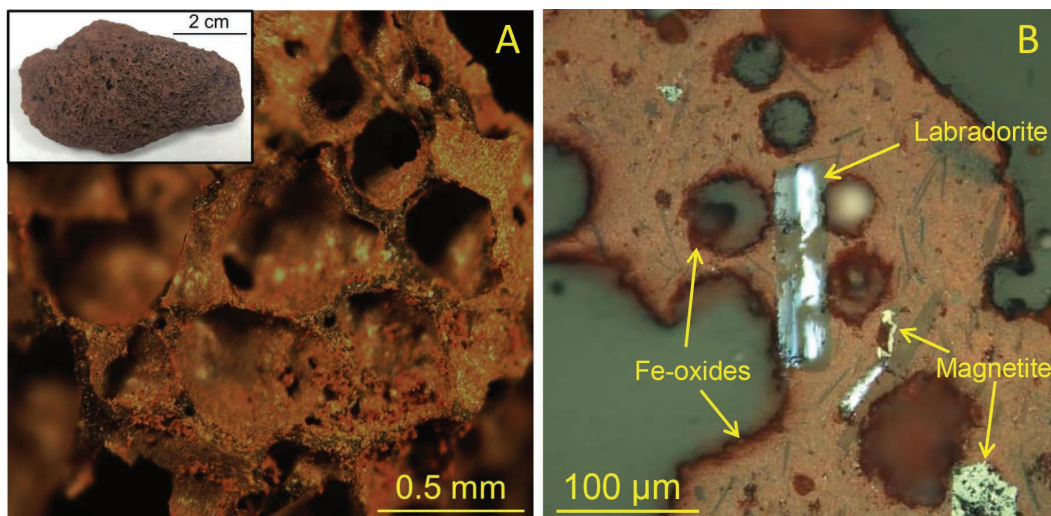


FIGURE 1. (a) A scoria hand specimen showing the porous texture with vesicles covered by reddish and brownish Fe-oxides of luogufengite, hematite, and maghemite. (b) A polished surface of a scoria thin section shows coating of the oxides on the vesicles' surfaces. Glassy groundmass of the scoria contains crystals of magnetite and platy labradorite minerals. The image was recorded under the reflected light mode. (Color online.)

tion during explosive eruptions of basaltic lava. Luogufengite formed during the formation of scoria at high temperature. Oxidation of Fe-bearing semi-plastic glass at high temperature resulted in the formation of ferric Fe-oxides of luogufengite on surfaces of the vesicles associated with maghemite and hematite (Fig. 1).

The sample for powder X-ray diffraction was carefully scratched off from the vesicles' surfaces within the collected basaltic scoria (Fig. 1). The silicate glass was removed by dissolving the sample in a 10M NaOH solution at 80 °C for 2 days following procedures for enriching synthetic $\epsilon\text{-Fe}_2\text{O}_3$ prepared at high temperature (Gich et al. 2006; Namai et al. 2009). The luogufengite crystals were enriched using a weak magnetic bar. High-resolution powder XRD data were collected at beamline 11-BM of the Advanced Photon Source (APS), Argonne National Laboratory. Diffraction patterns were recorded using a wavelength (λ) of 0.414125 Å. Sample powders were loaded into a Kapton capillary tube that was spun continuously at 5600 rpm during data collection to minimize preferred orientation. Data were collected from 0.5 to 50° 2 θ in steps of 0.001° at a scan speed of 0.01°/s. The instrument has a resolution of ~0.007° for the 2 θ range used in the structural refinement (2 θ : 3–25°), based on measured Cagliotti parameters using a LaB₆ standard (NIST SRM 660a) (Supplementary Fig. S1)¹. The X-ray beam size at the sample is ~1.5 mm (horizontal) × 0.5 mm (vertical).

The obtained synchrotron XRD data were analyzed using the Rietveld method with the Jade 9.0 program. The starting structural parameters were taken from the study of a synthetic $\epsilon\text{-Fe}_2\text{O}_3$ (Gich et al. 2005). A pseudo-Voigt peak-shape function was used for fitting the peak profiles. The peaks at 5.34–5.41°, 6.79–6.87°, 8.45–8.54°, 9.26–9.34°, 11.65–11.76°, and 14.16–14.28° belong to an unknown phase and were thus excluded for the refinement. Our TEM-EDS measurements on luogufengite reveal a total Fe and Al occupancy of $\text{Fe}_{3.53}\text{Al}_{0.47}$. Previous study on synthetic $\epsilon\text{-Al}_x\text{Fe}_{2-x}\text{O}_3$ (Namai et al. 2009) shows that Al prefers the Fe3 and Fe4 sites at ~10 at%. The ratio of Al occupancies at the Fe3 and Fe4 sites is sensitive to the intensity ratio of $I_{(011)}/I_{(022)}$ of luogufengite, based on simulated XRD patterns. Slight differences in Al occupancies at the Fe3 and Fe4 sites were determined from matching in the intensity ratio of $I_{(011)}/I_{(022)}$ between the observed and simulated XRD patterns.

Other XRD patterns were collected using a Rigaku Rapid II XRD system (MoK α radiation) in the Geoscience Department, University of Wisconsin-Madison. Diffraction data were recorded on a 2D image-plate detector. The original two-dimensional diffraction rings were then converted to produce conventional 2 θ vs. intensity patterns using Rigaku's 2DP software.

HRTEM imaging, X-ray energy-dispersive spectroscopy (EDS), and selected-area electron diffraction (SAED) analyses were carried out using a

Philips CM200-UT microscope equipped with GE light element energy-dispersive X-ray spectroscopy (EDS) at the Materials Science Center at the University of Wisconsin-Madison, and operated at 200 kV. Chemical analyses were obtained using the EDS (spot size 5 with a beam diameter of ~50 nm). Quantitative EDS results were obtained using experimentally determined k -factors from standards of albite, forsterite, anorthite, orthoclase, labradorite, fayalite, and titanite (see Table¹ S1 in Supplementary Material) (Hill 2009).

RESULTS AND DISCUSSION

The synchrotron XRD pattern shows that luogufengite is the dominant phase in a treated scoria sample, together with hematite, quartz, hydronium jarosite, and an unknown phase (Fig. 2). A trace amount of calcite originates from the paly-dough that was used for sealing the capillary tube. The XRD data with MoK α radiation also shows a similar pattern, except for the calcite peaks (Supplementary Fig. S2)¹. The (011), (002), (022), (013), (131), (004), and (135) peaks of luogufengite do not overlap with other diffraction peaks from coexisting minerals, although the strongest (122) peak of luogufengite is overlapped with the (014) peak of hematite (Fig. 2). The synchrotron XRD pattern of luogufengite shows the broad peaks with a full-width at half maximum (FWHM) of ~0.11°, (Table 1), indicating the nanometer sizes of the crystals (Fig. 2). Diffraction peaks from hematite are sharper than those from luogufengite. Likewise, diffraction peaks from quartz are much sharper than peaks from other phases. Diffraction peaks with “?” marks are from an un-identified phase. Its FWHM is very similar to that of hematite (Table 1).

The nano-crystals of luogufengite, maghemite, and hematite were identified using HRTEM, fast Fourier transform (FFT) patterns, and selected-area electron diffraction (SAED) patterns (Fig. 3). The diameter of luogufengite ranges from ~20 to ~120 nm (Fig. 3a). Hematite crystals are generally larger than luogufengite crystals, whereas maghemite crystals are smaller than luogufengite crystals (Fig. 3b). HRTEM images show that luogufengite commonly displays {100}, {010}, {00 $\bar{1}$ }, {011}, and $\{1\bar{1}1\}$ forms (Figs. 3c and 3d). Synthetic $\epsilon\text{-Fe}_2\text{O}_3$ crystals

¹Deposit item AM-17-45849, CIF/Supplemental Material. Deposit items are free to all readers and found on the MSA web site, via the specific issue's Table of Contents (go to http://www.minsocam.org/MSA/AmMin/TOC/2017/Apr2017_data/Apr2017_data.html).

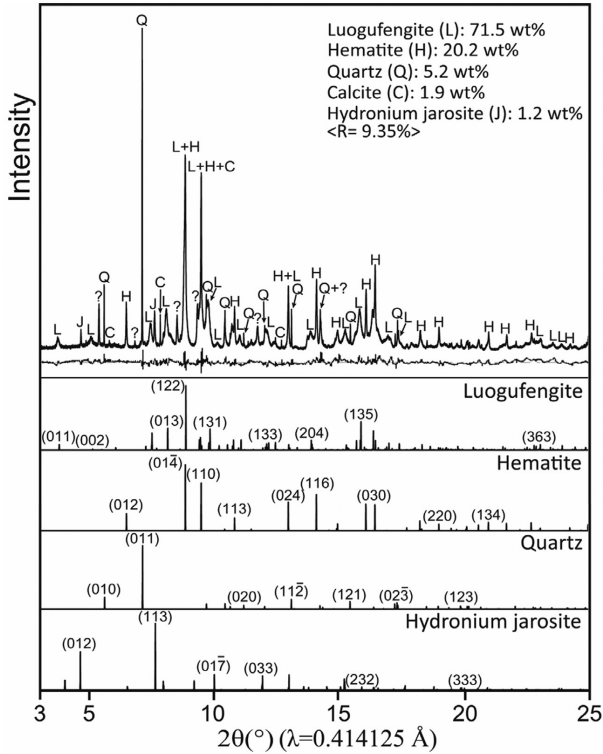


FIGURE 2. The synchrotron XRD pattern shows diffraction peaks from luogufengite (dominant), hematite, quartz, hydronium jarosite, and an unidentified phase. Diffraction peaks from luogufengite, hematite, quartz, and hydronium jarosite are marked below the XRD pattern. Percentages of these phases were calculated using the Rietveld method. A trace amount of calcite is from the platy-dough used for sealing the capillary tube. Peaks with “?” marks are from an un-identified phase. Their peak width (FWHM) is very similar to that of hematite. The refinement was conducted using the XRD pattern with the peaks from the unknown phase removed. The residual between measured and calculated patterns is illustrated right below the XRD pattern.

similarly display $\{100\}$, $\{01\bar{1}\}$, and $\{011\}$ crystallographic forms (Jin et al. 2004; Lee and Xu 2016). The rod shape of luogufengite is elongated along the a -axis (Fig. 3d). The ideal shape of luogufengite nano-mineral is constructed based on its symmetry and HRTEM images (Fig. 4).

The chemical formulas for luogufengite ($\text{Fe}_{1.71}\text{Al}_{0.24}\text{Mg}_{0.02}\text{Ti}_{0.03}\text{O}_3$), maghemite ($\text{Fe}_{1.69}\text{Al}_{0.25}\text{Mg}_{0.04}\text{Ti}_{0.02}\text{O}_3$), and hematite ($\text{Fe}_{1.76}\text{Al}_{0.02}\text{Mg}_{0.03}\text{Ti}_{0.19}\text{O}_3$) are calculated from X-ray EDS spectra (Fig. 5; Table 2). The luogufengite and maghemite nano-crystals contain small amounts of Al because the smaller Al^{3+} (compared with Fe^{3+}) prefers the tetrahedral Fe^{3+} site (Namai et al. 2009; Tucek et al. 2010), whereas, coexisting hematite crystals contain small amounts of Ti (Fig. 5; Table 2).

Large grains of luogufengite have (110) or $(\bar{1}10)$ twinning with composition planes of (130) and (100) due to the pseudo-hexagonal symmetry of its crystal structure (Fig. 6a). The relationship between the (110) twins is illustrated in Figures 7a and 7b. The observed twinning is very similar to the (110) twinning in aragonite. The $\sim 120^\circ$ rotational relationship between (010) and (110) and the displacement along the $b/3$

TABLE 1. The d -values, intensities and FWHMs of selected peaks (hkl) as well as crystallite size/strain analyses of observed minerals in the vesicles' coating layers

Phase	(hkl)	d (Å)	I_{obs}	FWHM 2θ (°)
Luogufengite	(011)	6.387	3.657	0.106(5)
	(002)	4.694	3.752	0.099(4)
	(022)	3.196	7.922	0.098(6)
Crystallite size (nm) = 38.8(4.9); strain (%) = 0.102(55)				
Hematite	(012)	3.673	14.575	0.034(4)
	(113)	2.2	13.117	0.035(7)
	(116)	1.689	21.592	0.039(5)
Crystallite size (nm) = 107.7(24.5); strain (%) = 0.042(33)				
Quartz	(010)	4.256	20.108	0.011(4)
	(011)	3.343	100	0.013(6)
	(211)	1.542	14.021	0.013(5)
Crystallite size (nm) = 832.5(109.1); strain (%) = 0.027(5)				
Hydronium jarosite	(012)	5.105	6.262	0.021(3)
Unknown		4.42	14.305	0.029(1)
		3.487	2.564	0.031(3)
		2.795	10.567	0.034(2)

Notes: Unit-cell parameters for quartz: $a_h = 4.91532(8)$, $c_h = 5.40604(11)$ Å. For hematite: $a_h = 5.02217(7)$, $c_h = 13.70852(27)$ Å. For hydronium jarosite: $a_h = 7.2916(1)$, $c_h = 17.5571(4)$ Å. The instrumental resolution: 0.007° (see Supplementary¹ Fig. S1 for details).

are also observed in the luogufengite nano-crystal (Fig. 6b). The relationship is illustrated in Figure 7c. The observed twin relationships are similarly identified in the synthetic ϵ -Fe₂O₃ crystals (Ding et al. 2007; Lee and Xu 2016).

Rietveld refinement was performed to derive the structural parameters of luogufengite on the basis of the determined space group $Pna2_1$ (Gich et al. 2005). Fractional coordinates and site occupancies are listed in Table 3. The unit-cell parameters of luogufengite are very similar to those of synthetic Al-bearing ϵ -Fe₂O₃ (Fig. 8). The slightly larger a dimension may be related to a small amount of Mg^{2+} in luogufengite. Table 4 lists the powder XRD data of luogufengite.

The structure of luogufengite contains three octahedra (denoted Fe1, Fe2, and Fe4 sites) and one tetrahedron (denoted as Fe3) (Fig. 9), and the structure is polar, which is associated with its magnetic properties. The average bond distance (1.831 Å) between oxygen and tetrahedral coordinated (Fe,Al) is slightly shorter than that in a synthetic ϵ -Fe₂O₃ structure (1.879 Å) (Fig. 10). The Fe1 and Fe2 site are shown in the distorted Fe octahedra, whereas the Fe4 sites are less distorted (Fig. 10). These distortions in the Fe sites of luogufengite are responsible for a non-zero orbital component of the total Fe^{3+} magnetic moment (Gich et al. 2005; Tucek et al. 2010).

Luogufengite is a Fe₂O₃ polymorph that is considered as an intermediate phase between maghemite (γ -Fe₂O₃) and hematite (α -Fe₂O₃) (Zboril et al. 2002; Sakurai et al. 2009; Lee and Xu 2016). Oxygen atoms in luogufengite display the doubled hexagonal (ABAC) packing, whereas oxygen atoms in maghemite and hematite have the cubic closest (ABC) and hexagonal (AB) packings, respectively. Specific gravities (g/cm^3) for end-member maghemite, synthetic ϵ -Fe₂O₃, and hematite are 5.07, 5.01, and 5.27, respectively. Thus, the phase transformations from γ -Fe₂O₃ \rightarrow ϵ -Fe₂O₃ and ϵ -Fe₂O₃ \rightarrow α -Fe₂O₃ involve changes in packing of oxygen atoms. New experimental results from annealing nontronite at high temperatures indicate that the stability of luogufengite in an amorphous silica matrix is size-dependent (Lee and Xu 2016) (Fig. 11). Sizes of luogufengite

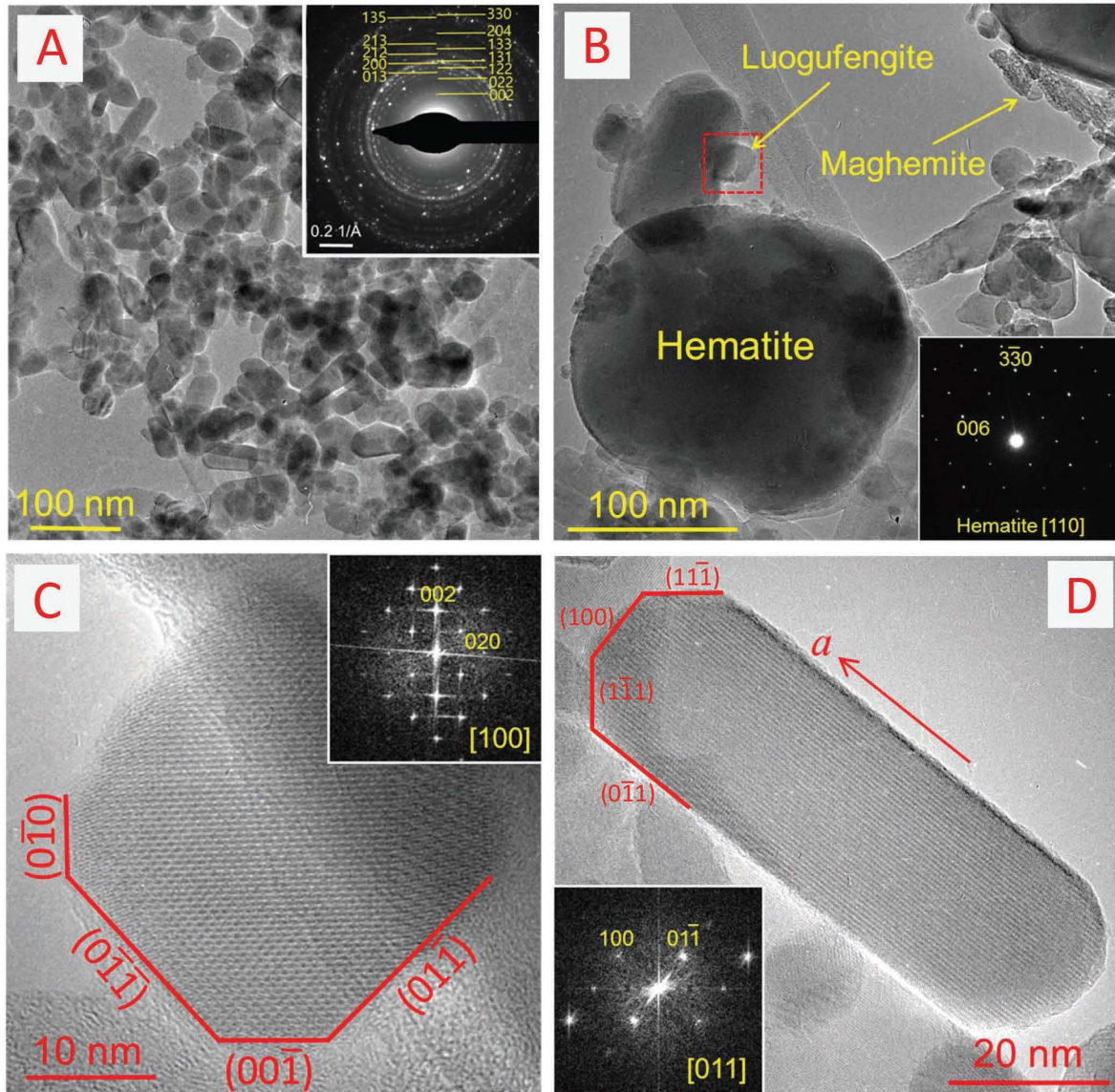


FIGURE 3. (a) Bright-field TEM images showing aggregated luogufengite with an inserted SAED pattern. (b) Bright-field TEM image shows that hematite crystals are generally larger than luogufengite, whereas maghemite crystals are generally smaller than luogufengite. (c) An HRTEM image and its FFT pattern (inserted at the up-right corner) showing single luogufengite nano-crystals from the outlined area in b. (d) An HRTEM image of the rod-shape of luogufengite elongated along the *a*-axis. (Color online.)

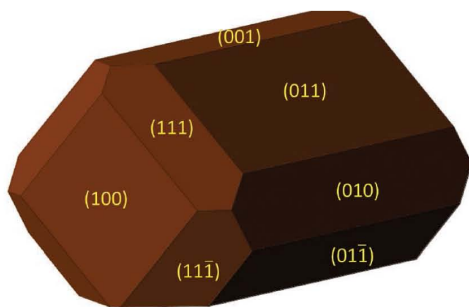


FIGURE 4. Proposed ideal morphology for luogufengite nano-mineral based on HRTEM images. (Color online.)

crystals may range from ~10 to ~200 nm in the amorphous silica matrix. Further growth of luogufengite will result in phase transformation to hematite. Synthetic luogufengite was also discovered in ancient Chinese black-glazed Jian wares, which formed at ~1300 °C (Dejoie et al. 2014). Therefore, the formation mechanism of luogufengite suggests a high-temperature condition coupled with a fast cooling history, an environment similar to that of an explosive volcanic eruption.

IMPLICATIONS

Luogufengite is an important mineral for understanding the paleomagnetism of volcanic rocks because of its unusual magnetic property. Paleomagnetism requires magnetic minerals to

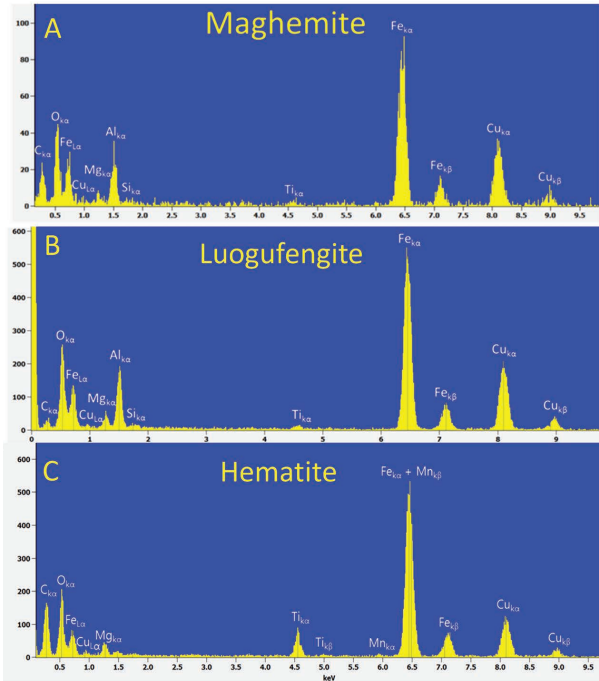


FIGURE 5. Representative X-ray EDS spectra from (a) maghemite, (b) luogufengite, and (c) hematite nano-minerals. Cu peaks are from the lacey carbon-coated copper grid that holds the TEM specimen. (Color online.)

TABLE 2. Chemical compositions of luogufengite, maghemite, and hematite

	(1)	(2)	(3)	(4)	(5)	Average
Luogufengite (Fe_{1.71}Al_{0.24}Mg_{0.02}Ti_{0.03}O₃)						
Fe ₂ O ₃ (wt%)	90.03%	89.74%	89.76%	90.18%	90.01%	89.94%
Al ₂ O ₃	7.84%	8.68%	8.01%	7.62%	7.48%	7.93%
MgO	1.06%	1.06%	1.73%	0.80%	1.46%	1.22%
TiO ₂	1.07%	0.52%	0.50%	1.40%	1.05%	0.91%
Fe	1.70	1.70	1.71	1.71	1.71	1.71
Al	0.23	0.26	0.24	0.23	0.22	0.24
Mg	0.02	0.02	0.03	0.02	0.03	0.02
Ti	0.05	0.02	0.02	0.04	0.04	0.03
Maghemite (Fe_{1.69}Al_{0.23}Mg_{0.04}Ti_{0.02}O₃)						
Fe ₂ O ₃ (wt%)	88.04%	88.37%	89.41%	89.13%	89.54%	88.90%
Al ₂ O ₃	9.43%	8.36%	7.87%	8.44%	8.59%	8.54%
MgO	2.14%	2.50%	2.33%	2.14%	1.62%	2.14%
TiO ₂	0.39%	0.77%	0.39%	0.29%	0.25%	0.42%
Fe	1.67	1.68	1.71	1.70	1.70	1.69
Al	0.28	0.25	0.24	0.25	0.26	0.25
Mg	0.04	0.05	0.04	0.04	0.03	0.04
Ti	0.01	0.03	0.01	0.01	0.01	0.02
Hematite (Fe_{1.76}Al_{0.02}Mg_{0.03}Ti_{0.19}O₃)						
Fe ₂ O ₃ (wt%)	92.85%	92.89%	92.71%	93.32%	93.04%	92.96%
Al ₂ O ₃	1.10%	0.42%	0.29%	0.78%	0.76%	0.67%
MgO	1.28%	1.20%	1.98%	1.09%	1.53%	1.42%
TiO ₂	4.77%	5.49%	5.02%	4.81%	4.67%	4.95%
Fe	1.76	1.76	1.76	1.77	1.77	1.76
Al	0.03	0.01	0.01	0.02	0.02	0.02
Mg	0.02	0.02	0.04	0.02	0.02	0.03
Ti	0.18	0.21	0.19	0.18	0.18	0.19

Note: All calculations are based on three oxygen atoms basis.

determine Earth’s ancient magnetic orientation relative to the magnetic poles at the time of rock formation. Remanent magnetism is detected in some rocks containing magnetic minerals such as magnetite and maghemite. Interestingly, luogufengite could be an important mineral for preserving the remanent

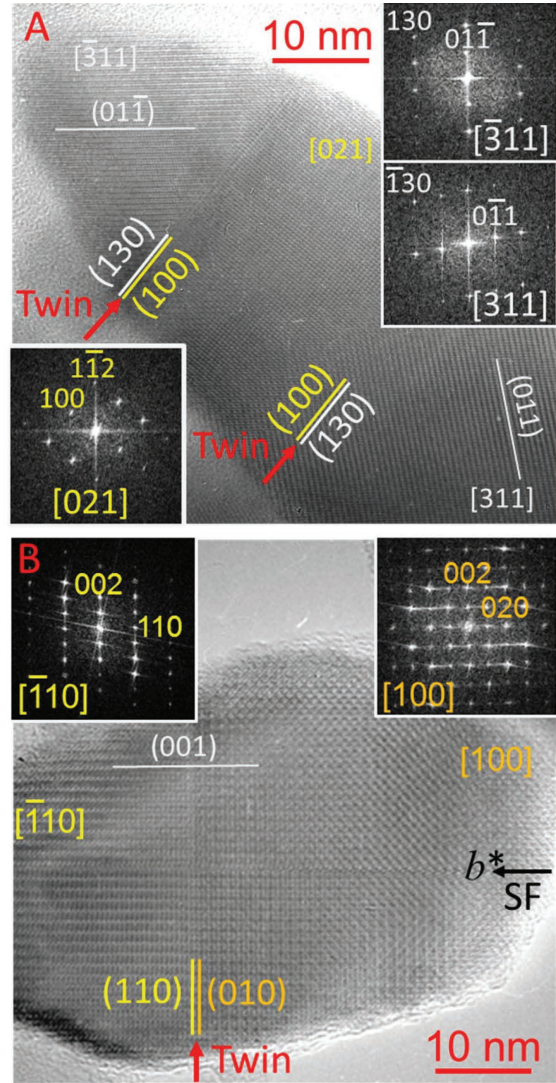


FIGURE 6. (a) An HRTEM image showing the luogufengite in a (110) twinning relationship. The composition planes are (130) and (100) due to its pseudo-hexagonal structure. The [311] zone-axis from one crystal is parallel to the [021] zone-axis of its twinned crystal. (b) An HRTEM image showing the composition plane boundaries between (110) and (010) of luogufengite and a stacking fault in a right side crystal. (Color online.)

magnetic property due to its large magnetic coercivity, the ability to withstand an external magnetic field. Thus, luogufengite is a promising mineral for paleomagnetism studies of volcanic rocks. Ordering of Al in the tetrahedral sites will enhance the magnetic property, because (001) layer with tetrahedra and the (001) layer without tetrahedra have opposite magnetic moments (Tucek et al. 2010; Yoshikiyo et al. 2012).

The mineral with its unique magnetic property may also explain the observed unusually high-remanent magnetization in some igneous and metamorphic rocks (Austin et al. 2014; Church et al. 2015; Rajagopalan et al. 1993; Foss and McKenzie 2011; Schmidt et al. 2007; Kuo et al. 2015), martian rocks (Acuna et al. 1999), and lodestones (natural magnet). It was proposed

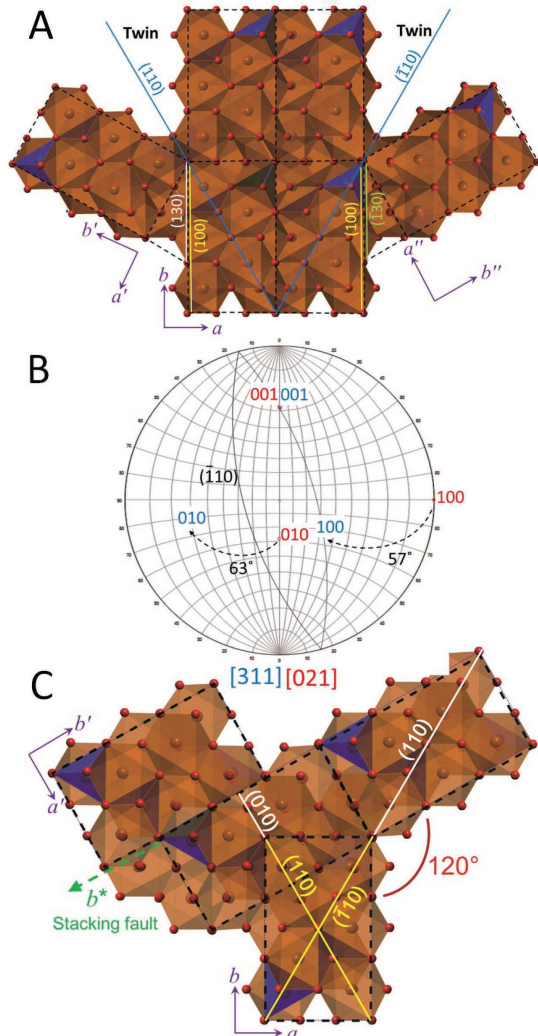


FIGURE 7. (a) Structure model showing the (011) twin relationship between the neighboring nano-crystals along the *c*-axis in Figure 6a. (b) Stereogram showing axial relationship between the twinned crystals in Figure 6. Red dots correspond to the axes of the right crystal in the model. Blue dots correspond to the axes of the center crystal in the model. (c) Structure model for Figure 6b showing $\sim 120^\circ$ rotation twin relationship with the displacement of $b/3$. (Color online.)

TABLE 3. Atomic coordinates of luogufengite (space group *Pna2*₁)

Atom	Occupancy	x	y	z
Fe1	Fe 1.00	0.1941(3)	0.1569(4)	0.5789(6)
Fe2	Fe 1.00	0.6844(5)	0.0228(3)	0.7893(7)
Fe3	Fe 0.73 Al 0.27	0.1878(3)	0.1531(6)	0.0000(2)
Fe4	Fe 0.80 Al 0.20	0.8081(4)	0.1602(2)	0.3044(6)
O1	O 1.00	0.9812(3)	0.3356(3)	0.4396(5)
O2	O 1.00	0.5106(2)	0.4953(3)	0.4154(5)
O3	O 1.00	0.6477(3)	0.9869(7)	0.1961(6)
O4	O 1.00	0.1569(5)	0.1568(6)	0.1902(3)
O5	O 1.00	0.8325(5)	0.1705(4)	0.6651(3)
O6	O 1.00	0.5391(4)	0.1717(2)	0.9423(6)

Notes: Lattice parameters: $a = 5.0647(3)$, $b = 8.7131(6)$, $c = 9.3842(5)$. Refinement agreement parameter: $R = 9.35\%$.

TABLE 4. Powder XRD data for luogufengite^a

l_{obs}	d_{obs}	d_{clac}	l_{clac}	hkl	l_{obs}	d_{obs}	d_{clac}	l_{clac}	hkl
7.6	6.3873	6.3852	9.4	011			1.9840	4.1	222
2.1	4.6944	4.6921	1.5	002	16.8	1.9727	1.9758	8.8	042
1.7	3.9694	3.9680	3.9	111			1.9682	3.7	203
4.8	3.3033	3.3028	6.1	120			1.9622	10.2	133
27.3	3.1965	{ 3.2013 7.8 112	7.3	1.9167	6.1	1.8386	1.9199	10.6	213
		{ 3.1926 27.0 022					1.8407	7.4	142
4.1	3.1167	3.1155	2.5	121			1.8348	2.8	015
29.1	2.9445	2.9441 35.4 013	2.8	1.7912			1.7937	3.5	223
100.0	2.7082	{ 2.7745 1.3 031					1.7251	1.0	115
		{ 2.7008 100.0 122	24.4	1.7155			1.7210	13.4	204
		{ 2.5453 15.7 113					1.7170	7.8	134
40.6	2.5343	{ 2.5324 19.2 200					1.7133	3.1	051
		{ 2.5195 6.9 130	6.9	1.5594			1.5628	6.5	312
		{ 2.4449 11.2 201					1.5577	2.9	242
35.8	2.4369	{ 2.4333 31.1 131	10.8	1.5208			1.5223	10.7	053
		{ 2.4317 3.1 210					1.5079	12.7	205
4.1	2.3421	2.3461 6.6 004					1.5051	36.7	135
7.8	2.2731	2.2711 7.9 123					1.4598	24.9	330
14.5	2.2231	{ 2.2285 5.9 202					1.4596	2.0	243
		{ 2.2197 14.9 132					1.4528	12.1	060
2.9	2.1793	2.1783 2.9 040	11.4	1.4051			1.4062	8.7	323
12.4	2.1558	2.1590 15.0 212					1.3959	1.6	160
1.9	2.0050	2.0011 2.9 140	7.7	1.3715			1.3728	8.1	252
			8.6	1.3028			1.3047	6.4	253

^aBold values are for the eight strongest peaks.

that the interface between cubic and rhombohedral phases may play an important role in remanent magnetization (McEnroe et al. 2001, 2002; Robinson et al. 2016). However, the exact role of the interfaces in enhancing this remanent magnetization is still not clear. The Fe-oxide minerals of magnetite with ilmenite exsolution lamellae or hematite with magnetite exsolution lamellae have luogufengite-like 2D crystals or domains with the doubled hexagonal packing at the interface between cubic and

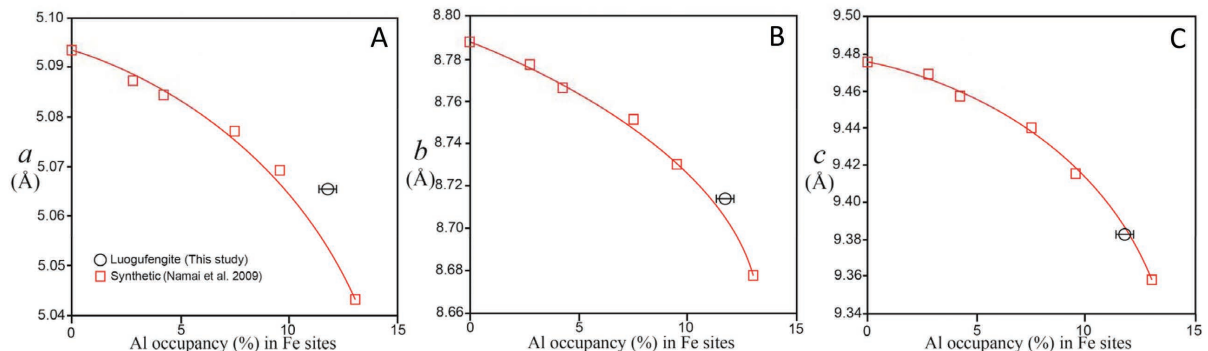


FIGURE 8. Comparisons of unit-cell parameters of luogufengite (black circle) and synthetic Al-bearing ϵ -Fe₂O₃ (red squares) (Namai et al. 2009). (Color online.)

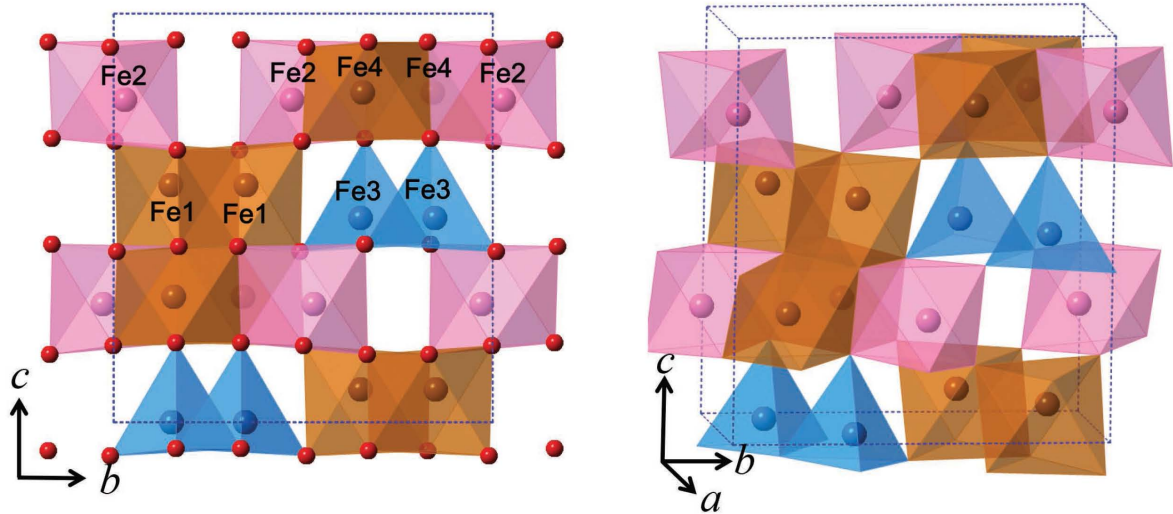
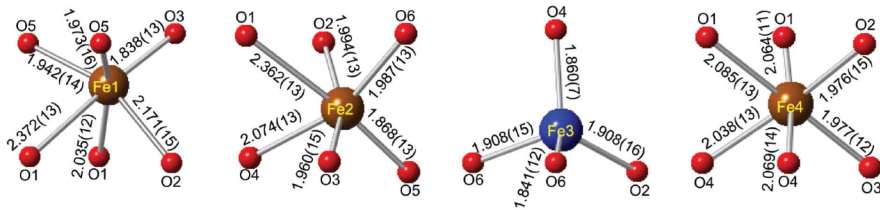


FIGURE 9. Polyhedral models showing the crystal structure of luogufengite. (Color online.)

Synthetic ε-Fe₂O₃ (Gich et al. 2006)



Luogufengite (This study)

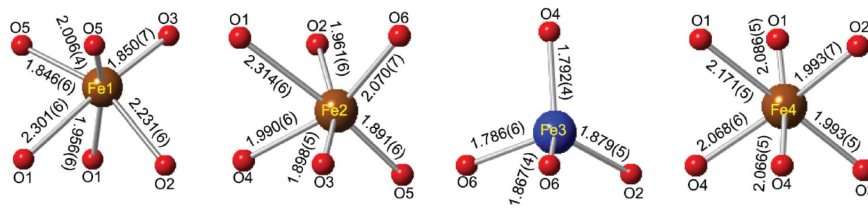


FIGURE 10. Bond distances for the polyhedra in synthetic pure ε-Fe₂O₃ (Gich et al. 2006) and luogufengite. The tetrahedra in the natural phase are slightly smaller than those in synthetic ε-Fe₂O₃. (Color online.)

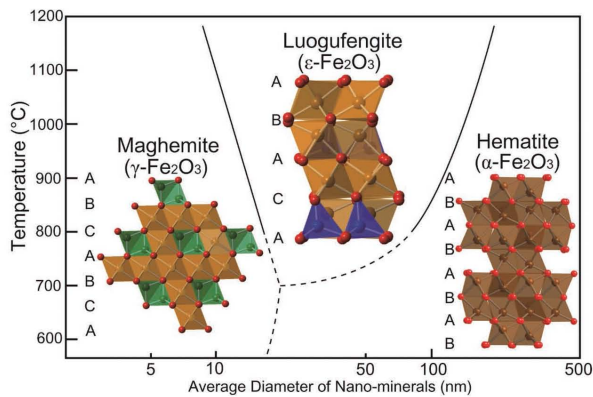


FIGURE 11. A size-dependent phase map of Fe³⁺ oxide polymorphs (modified from Lee and Xu 2016). (Color online.)

rhombohedral structures. The luogufengite-like nano-crystals or domains with the giant coercive fields at the interfaces could be an important reason for the unusually high-remanent magnetization of some rocks. Lodestones with large remanent magnetization are partially oxidized magnetite intergrown with maghemite and hematite (Banfield et al. 1994; Wasilewski and Kletetschka 1999; Kubo et al. 2015). Hematite lamellae or micro-precipitates in the magnetite host are evident in lodestone (Fig. 12a). Powder X-ray diffraction pattern of lodestone indicates that it is mostly of magnetite with small amount of maghemite and hematite (Fig. 12b). The quantitative analysis of mixture phase is calculated by Rietveld refinement from magnetite (Fleet 1986), maghemite (Shmakov et al. 1995), and hematite (Blake and Hessevick 1966) (Fig. 12b). Stacking faults in magnetite, maghemite, and hematite will result in luogufengite-like layer domains with the ABAC stacking locally. Luogufengite-like domains at the magnetite

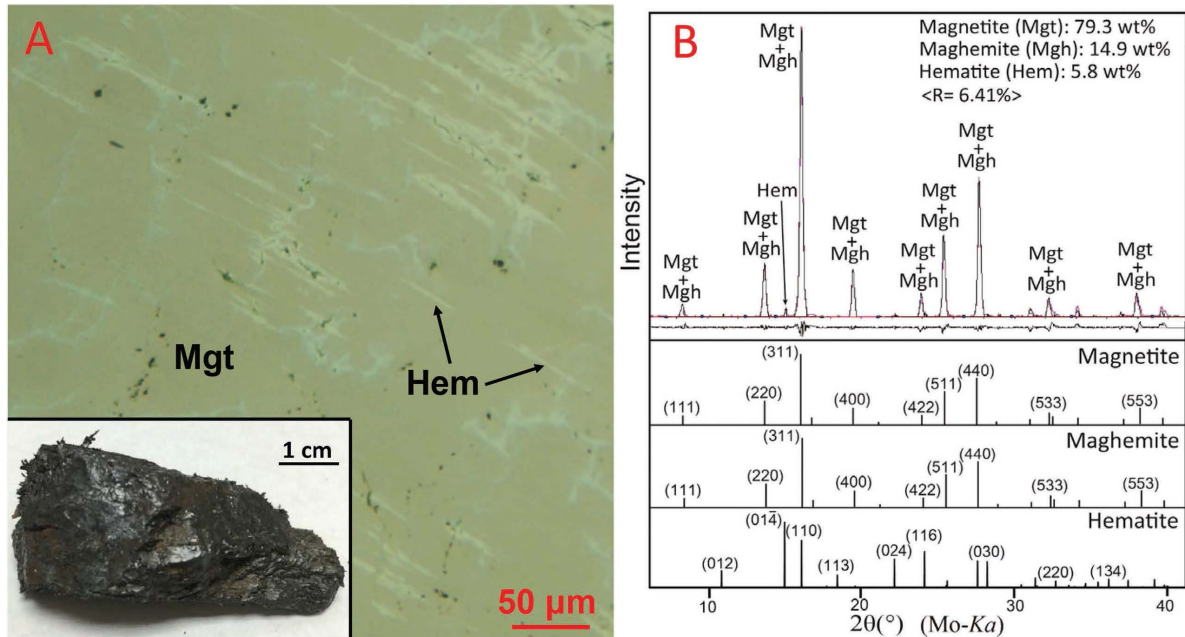


FIGURE 12. (a) A hand sample and optical microscope image of lodestone from Utah showing hematite lamellae in the magnetite host. The image was recorded under reflected light mode. (b) XRD pattern from the lodestone thin section. Percentages of mineral phases were calculated using the Rietveld method. The residual between the measured and calculated profiles is illustrated right below the XRD pattern. (Color online.)

and hematite/ilmenite interfaces are oriented nano-crystals. It is reported that oriented $\epsilon\text{-Fe}_2\text{O}_3$ nano-crystals along the a -axis will increase the coercive field when the external magnetic field is parallel to the a -axis (Sakurai et al. 2009). While magnetite and/or maghemite do not have large enough coercive fields (Dunlop and Özdemir 1997), luogufengite-like nano-domains at the magnetite/hematite interfaces might be responsible for the large coercive field of lodestones.

ACKNOWLEDGMENTS

This study was supported by the NASA Astrobiology Institute (N07-5489). Use of the Advanced Photon Source at Argonne National Laboratory was supported by the U.S. Department of Energy, Office of Science, Office of Basic Energy Sciences, under Contract No. DE-AC02-06CH11357. Los Alamos National Laboratory is operated by Los Alamos National Security LLC, under DOE Contract DE-AC52-06NA25396. We also thank Franklin Hobbs, Jun Wu, and an anonymous reviewer for providing many helpful suggestions.

REFERENCES CITED

- Acuna, M.H., Connerney, J.E., Ness, N.F., Lin, R.P., Mitchell, D., Carlson, C.W., McFadden, J., Anderson, K.A., Reme, H., Mazelle, C., Vignes, D., Wasilewski, P., and Cloutier, P. (1999) Global distribution of crustal magnetization discovered by the Mars Global Surveyor MAG/ER experiment. *Science*, 284, 790–793.
- Austin, J., Hillan, D., Schmidt, P.W., and Foss, C. (2014) Magnetism in the Giles complex. *Preview*, 171, 41–44.
- Banfield, J.F., Wasilewski, P.J., and Veblen, D.R. (1994) TEM study of relationships between the microstructures and magnetic properties of strongly magnetized magnetite and maghemite. *American Mineralogist*, 79, 654–667.
- Blake, R.L., and Hessevick, R.E. (1966) Refinement of hematite structure. *American Mineralogist*, 51, 123–129.
- Church, N., Austin, J., Schmidt, P.W., and McEnroe, S.A. (2015) Rock magnetic properties and mineral microstructure in high-remnance samples from ultramafic intrusions. 26th IUGG General Assembly, 22.06-07.09.15, Prague, Czech Republic.
- Dejoie, C., Sciau, P., Li, W.D., Noe, L., Mehta, A., Chen, K., Luo, H.J., Kunz, M., Tamura, N., and Liu, Z. (2014) Learning from the past: Rare epsilon- Fe_2O_3 in the ancient black-glazed Jian (Tenmoku) wares. *Scientific Reports*, 4, 4941.
- Ding, Y., Morber, J.R., Snyder, R.L., and Wang, Z.L. (2007) Nanowire structural evolution from Fe_3O_4 to epsilon- Fe_2O_3 . *Advanced Functional Materials*, 17, 1172–1178.
- Dunlop, D.J., and Özdemir, O. (1997) *Rock magnetism: Fundamentals and frontiers*. Cambridge Studies in Magnetism Series, 11, p. 573. Cambridge University Press, New York.
- Fleet, M.E. (1986) The structure of magnetite: symmetry of cubic spinels. *Journal of Solid State Chemistry*, 62, 75–82.
- Foss, C., and McKenzie, B. (2011) Inversion of anomalies due to remanent magnetisation: an example from the Black Hill Norite of South Australia. *Australian Journal of Earth Sciences: An International Geoscience Journal of the Geological Society of Australia*, 58, 391–405.
- Gich, M., Roig, A., Frontera, C., Molins, E., Sort, J., Popovici, M., Chouteau, G., Marero, D.M.Y., and Nogues, J. (2005) Large coercivity and low-temperature magnetic reorientation in epsilon- Fe_2O_3 nanoparticles. *Journal of Applied Physics*, 98, 044307.
- Gich, M., Frontera, C., Roig, A., Taboada, E., Molins, E., Rechenberg, H.R., Ardisson, J.D., Macedo, W.A.A., Ritter, C., Hardy, V., Sort, J., Skumryev, V., and Nogues, J. (2006) High- and low-temperature crystal and magnetic structures of epsilon- Fe_2O_3 and their correlation to its magnetic properties. *Chemistry of Materials*, 18, 3889–3897.
- Hackett, W.R., and Morgan, L.A. (1988) Explosive basaltic and rhyolitic volcanism of the eastern Snake River Plain. *Guidebook to the Geology of Central and Southern Idaho*, Idaho Geological Survey Bulletin, 283–301. Wiley, New York.
- Hill, T.R. (2009) High-resolution transmission electron microscopy investigation of nano-crystals of pyroxene and copper in Oregon sunstones. Master Thesis, University of Wisconsin-Madison.
- Jin, J., Ohkoshi, S., and Hashimoto, K. (2004) Giant coercive field of nanometer-sized iron oxide. *Advanced Materials*, 16, 48–51.
- Kohout, J., Brazda, P., Zaveta, K., Kubaniová, D., Kmjec, T., Kubicková, L., Klemetová, M., Santava, E., and Lancok, A. (2015) The magnetic transition in $\epsilon\text{-Fe}_2\text{O}_3$ nanoparticles: Magnetic properties and hyperfine interactions from Mössbauer spectroscopy. *Journal of Applied Physics*, 117, 17D505.
- Kubo, H., Nakamura, N., Kotsugi, M., Ohkochi, T., Terada, K., and Fukuda, K. (2015) Striped domains of coarse-grained magnetite observed by X-ray photoemission electron microscopy as a source of the high remanence of granites in the Vreddefort dome. *Frontiers in Earth Science*, 3, 31.
- Lee, S., and Xu, H. (2016) Size-dependent phase map and phase transformation kinetics for nanometric iron(III) oxides ($\gamma \rightarrow \epsilon \rightarrow \alpha$ pathway). *The Journal of Physical Chemistry C*, 120, 13316–13322.
- Machala, L., Tucek, J., and Zboril, R. (2011) Polymorphous transformations of nanometric iron(III) oxide: A review. *Chemistry of Materials*, 23, 3255–3272.
- McClellan, R.G., Schofield, M.A., Kean, W.F., Sommer, C.V., Robertson, D.P., Toth, D., and Gajdardziska-Josifovska, M. (2001) Botanical iron minerals: Correlation between nanocrystal structure and modes of biological self-assembly. *European Journal of Mineralogy*, 13, 1235–1242.

- McEnroe, S.A., Harrison, R.J., Robinson, P., Golla, U., and Jercinovic, M.J. (2001) Effect of fine-scale microstructures in titanohematite on the acquisition and stability of natural remanent magnetization in granulite-facies metamorphic rocks, southwest Sweden: Implications for crustal magnetism. *Journal of Geophysical Research*, 106, 523–30,546.
- McEnroe, S.A., Harrison, R.J., Robinson, P., and Langenhorst, F. (2002) Nano-scale haematite-ilmenite lamellae in massive ilmenite rock: An example of “lamellar magnetism” with implications for planetary magnetic anomalies. *Geophysical Journal International*, 151, 890–912.
- Namai, A., Sakurai, S., Nakajima, M., Suemoto, T., Matsumoto, K., Goto, M., Sasaki, S., and Ohkoshi, S. (2009) Synthesis of an electromagnetic wave absorber for high-speed wireless communication. *Journal of the American Chemical Society*, 131, 1170–1173.
- Rajagopalan, S., Schmidt, P.W., and Clark, D.A. (1993) Rock magnetism and geophysical interpretation of Black Hill Norite, South Australia. *Exploration Geophysics*, 24, 209–212.
- Robinson, P., McEnroe, S.A., Miyajima, N., Fabian, K., and Church, N. (2016) Remanent magnetization, magnetic coupling, and interface ionic configurations of intergrown rhombohedral and cubic Fe-Ti oxides: A short survey. *American Mineralogist*, 101, 518–530.
- Russell, W.J., and Brisbin, W.C. (1990) Primary fractures within a Tuff Cone, North Menan Butte, Idaho, U.S.A. *Journal of Volcanology and Geothermal Research*, 40, 11–22.
- Sakurai, S., Namai, A., Hashimoto, K., and Ohkoshi, S. (2009) First observation of phase transformation of all four Fe₂O₃ phases ($\gamma \rightarrow \epsilon \rightarrow \beta \rightarrow \alpha$ -phase). *Journal of the American Chemical Society*, 131, 18299–18303.
- Schmidt, P.W., McEnroe, S.A., Clark, D.A., and Robinson, P. (2007) Magnetic properties and potential field modeling of the Peculiar Knob metamorphosed iron formation, South Australia: An analog for the source of the intense Martian magnetic anomalies? *Journal of Geophysical Research*, 112, B03102.
- Shmakov, A.N., Kryukova, G.N., Tsybulya, S.V., Chuvilin, A.L., and Solovyeva, L.P. (1995) Vacancy ordering in gamma-Fe₂O₃—Synchrotron X-ray-powder diffraction and high-resolution microscopy studies. *Journal of Applied Crystallography*, 28, 141–145.
- Tronc, E., Chaneac, C., and Jolivet, J.P. (1998) Structural and magnetic characterization of ϵ -Fe₂O₃. *Journal of Solid State Chemistry*, 139, 93–104.
- Tucek, J., Zboril, R., Namai, A., and Ohkoshi, S. (2010) ϵ -Fe₂O₃: An advanced nanomaterial exhibiting giant coercive field, millimeter-wave ferromagnetic resonance, and magnetoelectric coupling. *Chemistry of Materials*, 22, 6483–6505.
- Tucek, J., Machala, L., Ono, S., Namai, A., Yoshikiyo, M., Imoto, K., Tokoro, H., Ohkoshi, S., and Zboril, R. (2015) Zeta-Fe₂O₃—A new stable polymorph in iron(III) oxide family. *Scientific Reports*, 5, 15091.
- Wasilewski, P., and Kleteschka, G. (1999) Lodestone: Natures only permanent magnet—What it is and how it gets charged. *Geophysical Research Letters*, 26, 2275–2278.
- Xu, H., and Lee, S. (2016) Luogufengite, IMA 2016-005. *CNMNC Newsletter No. 31* (June 2016), page 695; *Mineralogical Magazine*, 80, 691–697.
- Yoshikiyo, M., Yamada, K., Namai, A., and Ohkoshi, S. (2012) Study of the electronic structure and magnetic properties of ϵ -Fe₂O₃ by first-principles calculation and molecular orbital calculations. *The Journal of Physical Chemistry C*, 116, 8688–8691.
- Zboril, R., Mashlan, M., Krausova, D., and Pikal, P. (1999) Cubic β -Fe₂O₃ as the product of the thermal decomposition of Fe²⁺SO₄³⁻. *Hyperfine Interactions*, 120, 497–501.
- Zboril, R., Mashlan, M., and Petridis, D. (2002) Iron(III) oxides from thermal processes—synthesis, structural, and magnetic properties, Mössbauer spectroscopy characterization, and applications. *Chemistry of Materials*, 14, 969–982.

MANUSCRIPT RECEIVED MAY 10, 2016

MANUSCRIPT ACCEPTED NOVEMBER 1, 2016

MANUSCRIPT HANDLED BY ALEJANDRO FERNANDEZ-MARTINEZ